Angiogenesis (2013) 16:837–846
DOI 10.1007/s10456-013-9359-4

ORIGINAL PAPER

Quantitative positron emission tomography imaging of angiogenesis in rats with forelimb ischemia using ^{68}Ga-NOTA-c(RGDyK)

Joong Hyun Kim · Young-Hwa Kim · Young Joo Kim · Bo Yeun Yang · Jae Min Jeong · Hyewon Youn · Dong Soo Lee · Jae Sung Lee

Received: 24 March 2013 / Accepted: 10 June 2013 / Published online: 16 July 2013

Abstract Gallium-68-labeled 1,4,7-triazacyclononane-1,4,7-triacetic acid (NOTA)—cyclic Arg-Gly-Asp-$_D$-Tyr-Lys (c(RGDyK)) was developed for $\alpha_v\beta_3$ targeting, and is a promising agent for imaging of cancer and disorders related to angiogenesis. In this study, we performed kinetic analysis of ^{68}Ga-NOTA-c(RGDyK) in rats with surgically induced forelimb ischemia, and immunohistochemical analysis was also performed to assess $\alpha_v\beta_3$ immuno-staining level. Animal models were created by excision of the left brachial vessels, and a sham operation was performed on the right brachial region under 2 % isoflurane anesthesia. Using an animal positron emission tomography/computed tomography (PET/CT) scanner, a list mode PET scan (120 min) was started with the injection of ^{68}Ga-NOTA-c(RGDyK) via the tail vein at 3, 5 and 7 days after ischemic surgery. Volumes of interest were drawn on the left ventricle, sham operation, control, and ischemic regions. Compartmental and two graphical analyses (Logan and RE plots) were performed for kinetic parameter estimation. The immunohistochemical analysis was also performed after the last PET scan, and cell components were scored on a six point scale for quantification of immuno-staining level (0-negative to 5-very high). A 3-compartment model with reversible binding best described the tissue time-activity curves. The distribution volume of the ischemic region was significantly higher than that of the sham operation ($P < 10^{-6}$) and control region ($P < 10^{-9}$). Both the Logan and RE plots showed high correlation with compartmental analysis ($R^2 = 0.96$ and 0.95 for Logan and RE, respectively). The temporal changes in distribution volume and binding potential were not significant. The immuno-staining level of the ischemic region was significantly higher than that of sham operation ($P < 10^{-4}$) and control region ($P < 10^{-8}$). Kinetic modeling studies with dynamic ^{68}Ga-NOTA-c(RGDyK) PET scan are feasible based on an image-derived input function in a

Electronic supplementary material The online version of this article (doi:10.1007/s10456-013-9359-4) contains supplementary material, which is available to authorized users.

J. H. Kim · Y.-H. Kim · Y. J. Kim · B. Y. Yang · J. M. Jeong · H. Youn · D. S. Lee · J. S. Lee (✉)
Department of Nuclear Medicine, Seoul National University, Seoul, Korea
e-mail: jaes@snu.ac.kr

J. H. Kim
e-mail: jhkim419@gmail.com

J. H. Kim · B. Y. Yang · J. M. Jeong · D. S. Lee · J. S. Lee
Interdisciplinary Program in Radiation Applied Life Science, Seoul National University, Seoul, Korea

J. H. Kim · Y.-H. Kim · B. Y. Yang · J. M. Jeong · D. S. Lee · J. S. Lee
Institute of Radiation Medicine, Medical Research Center, Seoul National University, Seoul, Korea

Y.-H. Kim · J. S. Lee
Department of Biomedical Sciences, Seoul National University, Seoul, Korea

D. S. Lee
WCU Department of Molecular Medicine and Biopharmaceutical Science, Seoul National University, Seoul, Korea

J. S. Lee
WCU Department of Brain and Cognitive Sciences, Seoul National University, Seoul, Korea

rat ischemia model. The kinetic modeling analysis performed in this study will be useful for the quantitative evaluation of ^{68}Ga-NOTA-c(RGDyK) binding to $\alpha_v\beta_3$ in angiogenic tissues.

Keywords ^{68}Ga-NOTA-c(RGDyK) · Angiogenesis · Kinetic modeling · Positron emission tomography · Forelimb ischemia

Introduction

Angiogenesis is the physiological process involving the growth of new blood vessels, and is related to tumor progression and pathologic processes. Therefore, targeting angiogenesis is important for visualization and treatment of tumors and other disorders [1–3].

The cell surface glycoprotein $\alpha_v\beta_3$ is one of the cell surface receptors and prominent integrin members of activated endothelial cells that undergo angiogenesis and vascularization [4, 5]. Therefore, $\alpha_v\beta_3$ is highly expressed in the angiogenic region and associated with the tumor growth and metastasis [6, 7].

Cyclic Arg-Gly-Asp-$_D$-Tyr-Lys (c(RGDyK)) peptide is one of the most promising targeting agents specifically for $\alpha_v\beta_3$; therefore, it is being investigated intensively [7–9]. Several Arg-Gly-Asp (RGD) compounds labelled with various radioisotopes such as ^{125}I, ^{99m}Tc, ^{18}F, ^{90}Y, ^{111}In, ^{64}Cu, ^{89}Zr and ^{68}Ga have been developed for positron emission tomography (PET) or single photon emission computed tomography (SPECT) imaging [10–17]. Using these radio-pharmaceuticals, non-invasive imaging of humans and animals is possible. Recently, a 1,4,7-triazacyclononane-1,4,7-triacetic acid (NOTA)-based bi-functional chelating agent was developed to label a c(RGDyK) peptide with ^{68}Ga, in a straightforward manner at a high yield [18]. We also showed the high affinity of this tracer (^{68}Ga-NOTA-c(RGDyK)) for $\alpha_v\beta_3$ integrin and the feasibility for imaging angiogenesis in mice with induced hind limb hypoxia and in mice bearing tumor xenografts. In addition, we performed a whole-body distribution and radiation dosimetry study of ^{68}Ga-NOTA-c(RGDyK) in human subjects, which showed a rapid clearance, primarily via the renal pathway [19]. The effective dose and dose to the urinary bladder wall of this tracer were 22.4 μSv/MBq and 240 μGy/MBq, respectively, suggesting an acceptable range of radiation exposure to patients in clinical applications.

It should also be noted that the interest of ^{68}Ga-labeled tracers for clinical and preclinical PET has increased in recent years because of the favorable inherent physical properties of ^{68}Ga, such as an appropriate half-life (67.6 min), high positron yields (89 %) and accessibility by the use of an in-house ^{68}Ge/^{68}Ga generator [20, 21].

For the quantitative assessment of in vivo kinetic profile of ^{68}Ga-NOTA-c(RGDyK) binding to $\alpha_v\beta_3$ in an angiogenic region, a comprehensive kinetic modeling of the tracer is necessary. Several investigations on the kinetic modeling of RGD peptides labeled with ^{18}F and ^{64}Cu have been reported [22, 23], and there is a previous report on the kinetic analysis of ^{68}Ga-labeled PRGD2 peptides [16]. In this study, we performed kinetic analysis of ^{68}Ga-NOTA-c(RGDyK) PET studies in rats with surgically induced forelimb ischemia. The metabolic stability of ^{68}Ga-NOTA-c(RGDyK) was determined in blood samples of the rats through high performance liquid chromatography (HPLC) analysis. An optimized compartmental model was selected based on information theory, and two non-parametric graphical analysis methods (Logan and RE plot) describing reversible tracer binding were applied. The primary estimated kinetic parameters were the total and specific distribution volume of ^{68}Ga-NOTA-c(RGDyK) in the ischemic regions, which were compared to those in the sham operation region and control muscle. The immunohistochemical analysis was also performed after PET scan to assess $\alpha_v\beta_3$ immunostaining level of ischemic, sham operation and control regions.

Materials and methods

Radiochemistry

The radiopharmaceutical ^{68}Ga-NOTA-c(RGDyK) was prepared as described in previous works [18, 19]. Briefly, a NOTA-c(RGDyK) kit, which contains NOTA-c(RGDyK) (10.7 μg, 10 nmol), sodium acetate (49.0 μg, 0.6 mmol), and acetic acid (1.8 mg, 29 μmol), was prepared and used for ^{68}Ga labeling. Freshly eluted $^{68}GaCl_3$ (1.0 mL, ~740 MBq/0.1 M HCl solution) solution from a ^{68}Ge/^{68}Ga-generator was added to the NOTA-c(RGDyK) kit using a 24 gauge intravenous (IV) catheter and a fluorinated ethylene propylene (FEP) needle to avoid metal contamination. The reaction mixture was mixed vigorously, and kept at ~90–95 °C for 5 min. After the reaction, the reaction mixture was passed through an Alumina N light Sep-Pak® cartridge (Waters, MA, USA), which was pre-conditioned with water (5 mL), and syringe filter (0.2 μm Supor® Membrane Low protein binding, PALL Co.). Gallium-68-NOTA-c(RGDyK) was eluted with isotonic saline (2 mL). Radiochemical yields and purities were checked by radio-TLC; radiochemical yields were >98 % after the ^{68}Ga labeling procedure and radiochemical purities were >99.5 % after purification.

Animal model

All procedures of this study were approved by the Institutional Animal Care and Use Committee of the Medical Research Institute at the Seoul National University Hospital. In this study, thirteen Sprague–Dawley (SD) rats were used for kinetic analysis (SPF, male, 6–8 weeks old) and two SD rats were used for assessment of metabolic stability (SPF, male, 16 weeks old). The rats used for kinetic analysis were anesthetized by 2 % isoflurane during forelimb ischemic surgery. To induce unilateral forelimb ischemia, a horizontal incision was applied to the skin that covers the left brachial region. After the incision, the left brachial vessels were exposed and carefully separated. The brachial vessels were excised after ligation of the proximal and distal ends, and the skin was sutured [24]. For comparison, a sham operation was performed on the right brachial region. In the sham operation, the skin incision and the identification of the brachial vessels were performed, and the skin was closed.

PET/CT procedure

A dual-ring small-animal PET scanner (eXplore VISTA, GE Healthcare, Waukesha, WI, USA) was used in this study [25]. The scanner is composed of 2 rings of detector modules and each ring contains 18 detector modules. Each detector module has an area of 20×20 mm^2 and consists of a 13×13 array of dual-layer phoswich (front layer: Lutetium Yttrium Orthosilicate (LYSO); back layer: Gadolinium oxyorthosilicate (GSO)) scintillation crystals with dimensions of $1.45 \times 1.45 \times 7$ mm^3 for LYSO and $1.45 \times 1.45 \times 8$ mm^3 for GSO. The axial field of view (FOV) of the PET scanner is 48 mm including an 8 mm axial gap between the detector rings.

Rats were scanned 3, 5, and 7 days after the ischemic surgery to evaluate temporal changes of ^{68}Ga-NOTA-c (RGDyK) uptake. In all rat PET scans, the heart (left ventricle), sham operation, control, and ischemic regions were covered by an axial FOV (single bed position). To obtain the time-activity curves for these 4 volumes of interest (VOIs), list mode acquisition was performed over 120 min. Rats were maintained under 2 % isoflurane anesthesia during the PET/CT scans. The PET scan was started with an IV injection of ^{68}Ga-NOTA-c(RGDyK) via the tail vein (42.2 ± 2.5 MBq). Fifty-five dynamic frames (6×5 s, 3×10 s, 4×15 s, 16×30 s, 10×60 s, 10×240 s, 6×600 s) were generated from the 120 min list mode data. An X-ray CT transmission scan was performed after the 120 min PET scan to correct for gamma-ray attenuation and to obtain anatomical information.

All the dynamic frames were reconstructed using 2D ordered subset expectation maximization (OSEM) algorithm with 2 iterations and 16 subsets after scatter, attenuation, and normalization corrections and data rebinning. Reconstructed images had a dimension of $175 \times 175 \times 61$ with 0.3875 mm transaxial spacing and a 0.775 mm axial slice interval.

A calibration factor was obtained using a rat-sized uniform cylindrical phantom, which had a 50 mm diameter and 80 mm length. The calibration factor was used to convert the pixel count rate on emission PET images to activity per unit volume (kBq/ml).

Metabolism of ^{68}Ga-NOTA-c(RGDyK)

Two normal rats without ischemic surgery were intravenously injected with ^{68}Ga-NOTA-c(RGDyK). Approximately 2 mL of blood was sampled at 1 h after the injection of ^{68}Ga-NOTA-c(RGDyK) via the tail vein. Whole-blood samples were collected in a heparin-containing vacuum tube, and plasma samples were extracted after 5 min centrifugation at 10 °C (3,000 rpm). The plasma samples were deproteinated by addition of 1 mL of aliquot serum and 1 mL of 15 % TCA, and centrifugation at 25 °C (3,000 rpm, 5 min). The supernatants containing ^{68}Ga-NOTA-c (RGDyK) were passed through a 0.2 μm pore size low protein binding syringe filter and analyzed by HPLC.

The standard ^{68}Ga-NOTA-c(RGDyK) was also analyzed by HPLC, and the metabolite fraction of the plasma sample was estimated by a comparison with the HPLC profile of standard ^{68}Ga-NOTA-c(RGDyK).

Kinetic analysis

To obtain time-activity curves for kinetic analysis, VOIs were drawn on the left ventricle, sham operation, control and ischemic regions. About 23 μL of a high uptake region close to the left brachial region on summed emission PET images (from 20 to 120 min post injection) was selected as the ischemia VOI. The VOI of the sham operation and control regions were drawn on the right brachial region and latissimus dorsi muscle with a size identical to that of the ischemia VOI. A spherical VOI was drawn at the center of the left ventricle with a 2 mm diameter (35 μL) to obtain an image-derived plasma input function. The plasma tracer concentration ($C_P(t)$) was assumed to be twice the whole-blood concentration ($C_{WB}(t)$), because the uptake by blood cells of the c(RGDyK) is negligible and hematocrit was approximately 50 % of whole-blood in rats [23, 26].

$$\frac{C_{WB}(t)}{C_p(t)} = 0.5$$

For the kinetic analysis, a linear compartmental model was used in this study. Figure 1 shows a 3-compartment model in which, $C_P(t)$, $C_{ND}(t)$, and $C_S(t)$ represent the time-

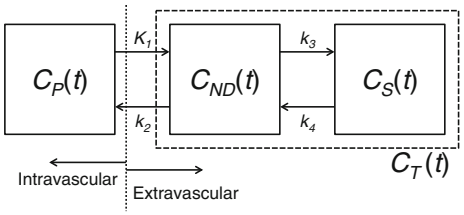

Fig. 1 Three-compartment model for reversible radiotracers

varying tracer concentration of the plasma, free or non-specific binding, and specific binding to $\alpha_v\beta_3$ integrin within the extravascular ischemic region, respectively. K_1, k_2, k_3 and k_4 represent the extravasation rate of the tracer, tissue efflux rate of free or non-specific binding tracer, the rate of specific binding of ^{68}Ga-NOTA-c(RGDyK) to the extracellular portion of the $\alpha_v\beta_3$ integrin and dissociation rate, respectively. The blood volume fraction (V_b) was also included in the compartmental model. Therefore, a total of five parameters were considered. Two kinds of model were evaluated to determine the optimal compartmental model: three-compartmental model and two-compartmental model. The three-compartmental model represents reversible $\alpha_v\beta_3$ integrin binding with five parameters (3C5P, K_1, k_2, k_3, k_4 and V_b), and the two-compartmental model combined nonspecific and specific binding compartments into a single tissue compartment with three parameters (2C3P, K_1, k_2 and V_b). Models with irreversible binding were not considered because of the obvious reversible characteristics of this tracer as shown in tissue time-activity curves.

Tissue time-activity curves were fitted to the models using a nonlinear least-squares method with the Levenberg–Marquardt algorithm, which minimizes the weighted sum of squared errors between PET measurements and model solutions. Inverse standard deviations of frame counts were used as the weights in the estimation. The Akaike information criterion (AIC) was used to determine the most appropriate model for ^{68}Ga-NOTA-c(RGDyK).

Binding potential (BP), total distribution volume (V_T) and the distribution volume for specific binding (V_S) of ^{68}Ga-NOTA-c(RGDyK) were calculated by the following equations:

$$BP = \frac{k_3}{k_4}$$

$$V_T = \frac{K_1}{k_2}\left(1 + \frac{k_3}{k_4}\right)$$

$$V_S = \frac{K_1 k_3}{k_2 k_4}.$$

Kinetic parameters obtained with a shorter scan duration were compared with those obtained with data acquired over 120 min.

Nonparametric graphical analyses, such as the Logan plot [27] and the relative equilibrium-based graphical plot (RE plot) [28, 29] were also performed to estimate V_T. Parametric images of V_T were obtained by applying both graphical methods. For all of the graphical analyses, we used 20 min as the starting point (equilibrium time) for linear regression of the dynamic PET studies because all graphs became linear after 20 min.

Immunohistochemical analysis

After the last PET scan, 6 of 13 rats were sacrificed for immunohistochemical analysis. Forelimb ischemic, sham operation, and control regions were fixed with 10 % neutral buffered formalin and embedded in paraffin. For $\alpha_v\beta_3$ immuno-staining, 4 mm-thick sections were obtained from paraffin blocks. Slides were incubated for 2 h at room temperature with mouse monoclonal $\alpha_v\beta_3$ antibody (NB600-1342, Novus Biologicals, Littleton, CO), and washed in PBS three times for 3 min. Then secondary antibody was applied and allowed to react for 45 min followed by washing in PBS. To amplify the signal of integrin $\alpha_v\beta_3$, the Vectastain Elite ABC kit® (Vector laboratories, Burlingame, CA) was used. Slides were counterstained with Mayers Hematoxylin (Electron Microscopy Sciences, Fort Washington, PA) and coated with Aquaperm® mounting media (Fisher). Slides were viewed on a Leica DMLB microscope (Leica Microsystems, Wetzlar, Germany) and photographed. To quantify the intensity of $\alpha_v\beta_3$ staining, cell compartments within sections were scored by two independent observers on a six point scale (0-negative, 1-very weak, 2-weak but clearly positive, 3-intermediate, 4-high, and 5-very high). All experiments were replicated at least three times for each animal on different days.

Results

Metabolic stability of ^{68}Ga-NOTA-c(RGDyK)

The metabolic stability of ^{68}Ga-NOTA-c(RGDyK) was determined in blood samples from two normal rats without ischemic surgery. Figure 2 shows the HPLC profiles of standard ^{68}Ga-NOTA-c(RGDyK), and blood samples from the rats taken 1 h after injection. For all profiles, a main peak was found around 10 min (10.0–10.2 min). The peak at 8 min present in the standard ^{68}Ga-NOTA-c(RGDyK) is believed to be a kind of isomers existing at a minor amount due to a 3-dimensional structure of a peptide derivative after labeling with ^{68}Ga. The HPLC patterns of blood samples did not change significantly from that of the standard ^{68}Ga-NOTA-c(RGDyK), which represents that no significant metabolism has occurred.

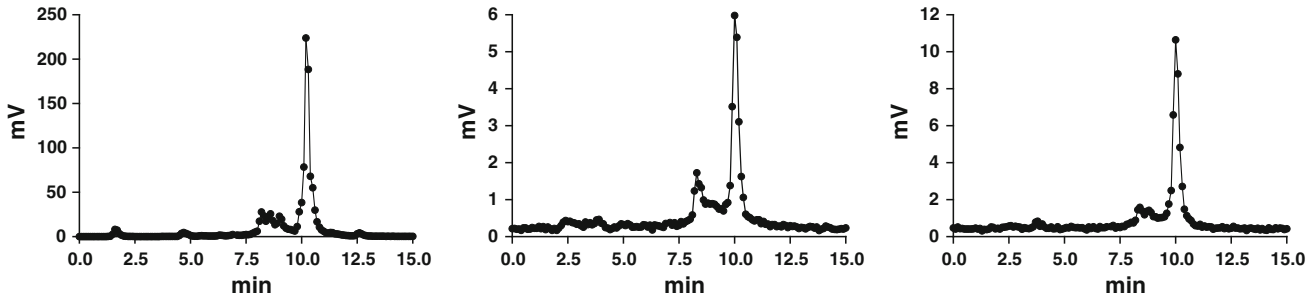

Fig. 2 HPLC profiles of standard ^{68}Ga-NOTA-c(RGDyK) (*left*) and blood samples of two normal healthy rats (*center* and *right*). The HPLC patterns of blood samples did not change significantly from that of the standard ^{68}Ga-NOTA-c(RGDyK)

Tissue time-activity curves

Two-hour dynamic PET scans were performed. Gallium-68-NOTA-c(RGDyK) was highly accumulated in the left brachial region where the ischemic surgery was performed. The mean tissue time-activity curves over all animals are shown in Fig. 3, which shows that the activity concentration of the ischemic region is higher than for the sham operation and control regions in all tested days. Supplementary Figure 1 shows that ^{68}Ga-NOTA-c(RGDyK) uptake in the ischemic region is 2–3 times higher than the control region. On the contrary, there was only a slight increase of ^{68}Ga-NOTA-c(RGDyK) uptake in the sham operation region relative to the control region.

Kinetic analysis

Table 1 shows the rate constants of the ischemic region obtained from the compartmental analysis. The *BP* was calculated from the 3C5P model. The root mean square error (RMSE) and AIC of 3C5P were lower than those of 2C3P. The quality of curve fitting (Fig. 4) also indicates that 3C5P is a more appropriate model than 2C3P for kinetic modeling of ^{68}Ga-NOTA-c(RGDyK) in the ischemic region.

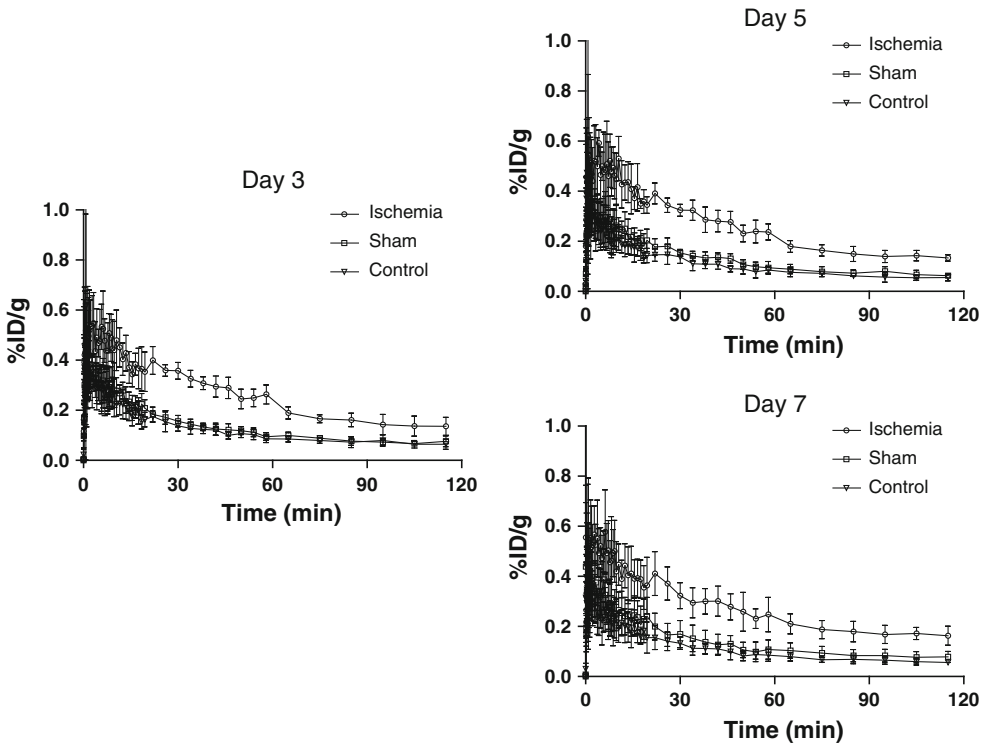

Fig. 3 Mean time-activity curves of rats. All curves decreased until the last scan. The activity concentration of the ischemic region was higher (about two times) than the sham operation and control region in all test days. The *error bar* represents standard deviation

Table 1 Kinetic parameters in the ischemic region obtained from compartmental analysis

Group	Model	K_1	k_2	k_3	k_4	V_b	RMSE	AIC	*BP*
Day 3 (n = 7)	2C3P	0.068 (36.9)	0.186 (43.7)			0.092 (22.5)	0.0036	−301.0	
	3C5P	0.104 (28.2)	0.456 (34.5)	0.068 (95.3)	0.046 (48.1)	0.069 (35.7)	0.0031	−306.5	1.328 (35.6)
Day 5 (n = 6)	2C3P	0.073 (37.6)	0.184 (53.7)			0.092 (29.8)	0.0034	−307.7	
	3C5P	0.104 (32.4)	0.317 (39.0)	0.041 (18.6)	0.038 (20.9)	0.074 (37.4)	0.0028	−313.0	1.087 (12.2)
Day 7 (n = 8)	2C3P	0.070 (33.6)	0.191 (33.2)			0.083 (55.9)	0.0038	−303.1	
	3C5P	0.132 (72.1)	0.576 (83.7)	0.048 (104.6)	0.030 (87.5)	0.055 (93.4)	0.0029	−315.0	1.443 (30.9)

Data are presented as mean (CV)

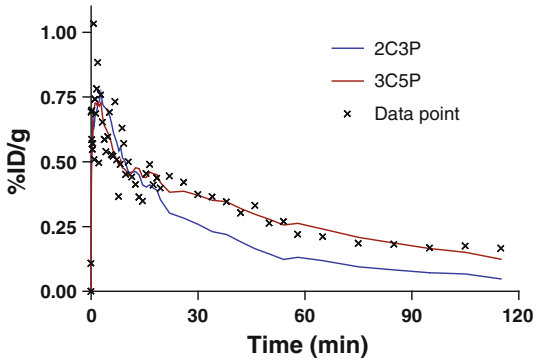

Fig. 4 Quality of curve fitting for a representative time-activity curve obtained from the ischemic region of a rat. The regression curve of the 3C5P (*red*) model was much closer to the data point than the 2C3P model (*blue*). (Color figure online)

Figure 5 shows the Logan and RE plots of a representative case in which the slope of each data set equals to V_T. Table 2 shows the V_T and the V_S of the ischemic, sham and control regions calculated from the compartmental analysis and two graphical analyses. The distribution volumes of the compartmental analysis showed a higher coefficient of variation than those of the graphical analyses. The V_T from the RE plot was slightly lower than that obtained from the Logan plot. Figure 6 shows parametric images of V_T using both graphical approaches. High V_T voxels were shown in the ischemia area for both parametric images. The parametric images of the Logan and RE plots show similar results as shown in the results of the organ-based approach (Table 2). Figure 7 shows a correlation of V_T of compartmental analysis (3C5P) with graphical analyses. Both the Logan and RE plots show a high correlation with compartmental analysis ($R^2 = 0.96$ and 0.95 for Logan and RE, respectively).

Tables 1 and 2 show that the temporal changes in V_T and *BP* were not significant over 5 days of serial scanning. In Table 3, the V_T and V_S values obtained using the 3C5P model and shorter scan duration were compared with those obtained with data acquired over 120 min, illustrating the feasibility of PET scans with a shorter scan duration with less than 5 % mean difference from those obtained with the 120-min 3C5P model.

Immunohistochemical analysis

In forelimb ischemic, sham operation, and control region, different patterns of staining level of integrin $\alpha_v\beta_3$ were observed. The ischemic region had the strongest $\alpha_v\beta_3$ staining signal, however, the control region had an almost undetectable level of the signal. The quantified intensity scores of $\alpha_v\beta_3$ staining were 1.4 ± 0.6, 2.4 ± 1.1 and 4.3 ± 0.7 for control, sham operation and ischemic region, respectively (Fig. 8).

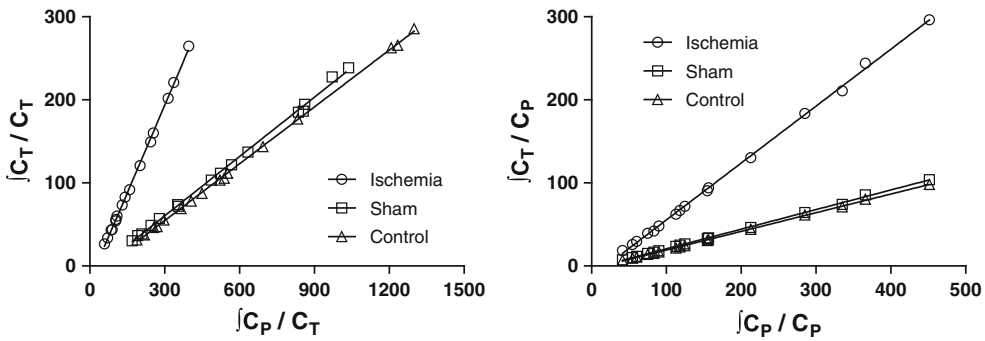

Fig. 5 Logan (*left*) and RE plots (*right*) of a representative case in which the slope of each data equals to V_T

Table 2 Distribution volumes obtained from compartmental analysis, Logan plot and RE plot

Group	Region	Compartment model (3C5P)		Logan plot	RE plot
		V_T	V_S	V_T	V_T
Day 3 (n = 7)	Ischemia	0.540 (13.8)	0.301 (15.6)	0.561 (9.0)	0.549 (8.4)
	Sham	0.335 (67.1)	0.208 (83.1)	0.279 (13.4)	0.274 (12.9)
	Control	0.226 (25.4)	0.117 (32.4)	0.257 (10.1)	0.253 (9.6)
Day 5 (n = 6)	Ischemia	0.590 (6.9)	0.306 (6.1)	0.613 (8.2)	0.600 (7.9)
	Sham	0.288 (18.4)	0.155 (19.8)	0.299 (17.0)	0.293 (15.7)
	Control	0.254 (42.6)	0.137 (74.3)	0.251 (9.7)	0.247 (9.1)
Day 7 (n = 8)	Ischemia	0.629 (21.2)	0.365 (27.7)	0.579 (15.2)	0.556 (14.6)
	Sham	0.291 (31.7)	0.152 (43.9)	0.284 (19.1)	0.279 (18.5)
	Control	0.197 (11.4)	0.095 (21.3)	0.229 (13.6)	0.225 (13.2)

Data are presented as mean (CV)

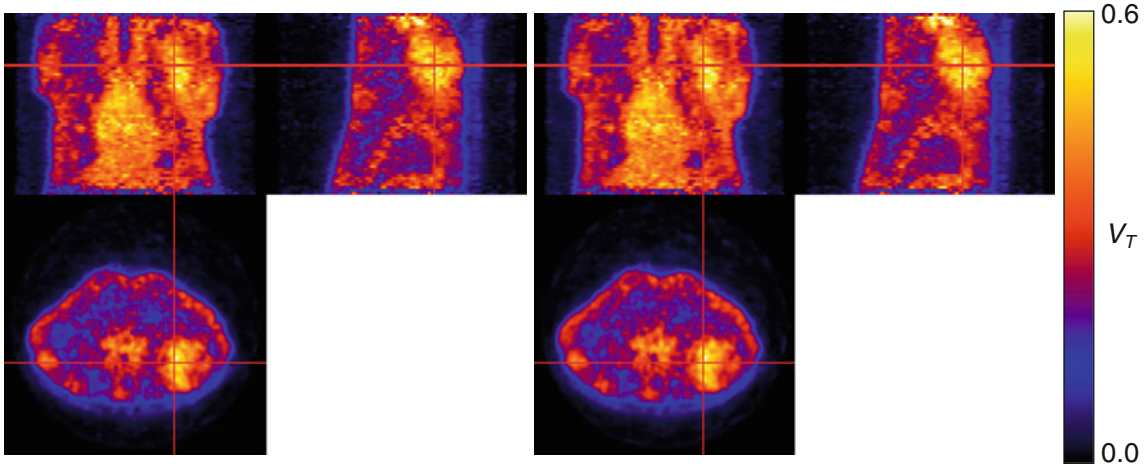

Fig. 6 Parametric images obtained by the Logan (*left*) and RE (*right*) plot. High V_T voxels were found around the ischemic region

Discussion

Gallium-68 labeled NOTA-c(RGDyK) is a recently developed PET radiotracer for visualizing angiogenesis, and is a promising candidate for imaging cancer and several other disorders [10, 18–20]. The aim of this study was to evaluate the tracer kinetic model for quantifying ^{68}Ga-NOTA-c(RGDyK) uptake and binding in an animal model of angiogenesis. For this purpose, forelimb ischemic models were created in 13 SD rats, and two-hour dynamic PET studies were performed after an IV injection of ^{68}Ga-NOTA-c(RGDyK). Time-activity curves for the left ventricle and ischemic, sham, and control regions were obtained and employed for estimating rate constants and related kinetic parameters based on compartmental modeling and graphical analyses. The immunohistochemical analysis was applied to confirm the result from kinetic analysis.

The results of HPLC-based metabolite analysis (Fig. 2) confirmed that metabolism of c(RGDyK) was negligible. Accordingly, the plasma input function for kinetic modeling was obtained from the left ventricular blood pool activity under the assumption that there is a small inter-subject variation in rat hematocrit. Note that the kinetic parameters estimated in this study comprise such errors due to the assumption of identical hematocrit.

In this study, we did not apply partial volume or spill-over corrections to the left ventricular input function, because the left ventricle of rat was sufficiently larger than the VOI radius for the left ventricle (2 mm) and the spatial resolution of the PET scanner used. In our previous study for kinetic modeling of ^{18}F-FLT in a subcutaneous tumor model, we scaled the image-derived left ventricular input function using a recovery coefficient obtained by comparing PET and a blood sample data [30]. However, the animal used in our previous study was a mouse, and the

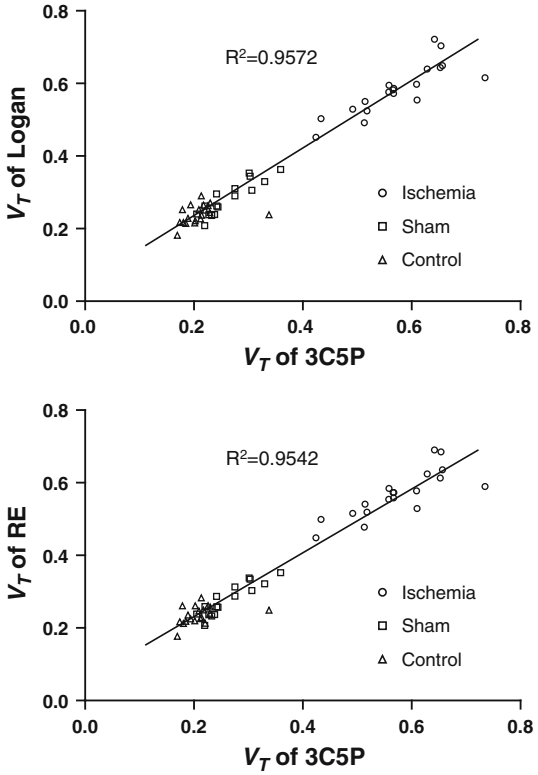

Fig. 7 Correlation of V_T of the Logan plot with the compartmental analysis (*top*) and RE plot with the compartmental analysis (*bottom*). Both of the graphical analyses show high correlation with the compartmental analysis

Table 3 Average percentage changes in total and specific binding distribution volume (V_T and V_S) of ^{68}Ga-NOTA-c(RGDyK) in the ischemic region obtained from the 3C5P model and 120 min data

Method	Mean ± SD % change	
	V_T	V_S
3C5P, 60 min	0.27 ± 18.22	1.73 ± 31.98
3C5P, 80 min	−2.75 ± 3.57	−3.62 ± 6.65
3C5P, 100 min	−2.36 ± 1.85	−3.34 ± 3.58

recovery coefficient for about a 2 mm VOI was almost 95 %. The subject was also a mouse in another study in which the partial volume correction was applied [23].

The size of the VOIs for the ischemic, sham, and control regions were only around 200 voxels (23 μL). This is the main reason for the statistical fluctuations shown in the tissue time-activity curves in Fig. 3 although they are the average curves of 6–8 rats. We did not apply larger VOIs despite the gain in counting statistics, because the larger VOIs may include normal voxels around the ischemic lesion, leading to a reduction of the contrast in kinetic parameters between the ischemic versus sham or control regions.

In this study, the 3-compartment model with irreversible binding (3C4P, $k_4 = 0$) was not evaluated because the tissue time-activity curves quickly reached the initial peak and decreased gradually until the last data point. Moreover, the quality of curve fitting with the 3C4P model was inadequate for all tissue regions. As shown in Fig. 4, a 3-compartment model with reversible radiotracer (3C5P) was more appropriate than a 2-compartment model (2C3P) for curve fitting of the time-activity curve of the ischemic region. This was also quantitatively confirmed by the AIC and RMSE values. This result indicates that the ^{68}Ga-NOTA-c(RGDyK) binds to the $\alpha_v\beta_3$ integrin reversely, and the 3-compartment with reversible binding model would be suitable for kinetic modeling of ^{68}Ga-NOTA-c(RGDyK). Time-activity curves were fitted more accurately when the blood volume fraction (V_b) was included in the model fitting. This indicates that the blood vessels would have significant volume in the ischemic region. The V_b occupies 5.5–7.4 % of the volume of the ischemic region (Table 1). However, the blood volume differences among the data acquired in 3 different days were not significant.

The graphical analysis methods yielded more robust results than the 3C5P compartmental analysis when the total distribution volumes (V_T) obtained from these methods were compared. On the other hand, the V_T values obtained using 3C5P and graphical analyses were highly correlated. The RE plot yielded a slightly lower V_T than the Logan plot in all data. The quality of the V_T parametric images generated using the Logan and RE methods were almost equivalent, indicating there is no significant improvement of image quality by applying RE plot.

Figure 3 shows the average time-activity curves presented in units of %ID/g. The uptake in the ischemic region at 20 min post-injection of ^{68}Ga-NOTA-c(RGDyK) is approximately 0.4 %ID/g and decreased continuously. As shown in Table 2, V_T in the ischemic region ranges between 0.54 and 0.63. Although there was a relatively low level of ^{68}Ga-NOTA-c(RGDyK) accumulation in the ischemic region, the V_T parametric images showed a remarkable contrast between the ischemic region and the sham or control regions, indicating the high specificity of ^{68}Ga-NOTA-c(RGDyK) binding to the target site (Fig. 6). These results were supported by immunohistochemical analysis. The immuno-staining level of the ischemic region (4.3 ± 0.7) was significantly higher than that of the sham operation (2.4 ± 1.1, $P < 10^{-4}$) and control region (1.4 ± 0.6, $P < 10^{-8}$).

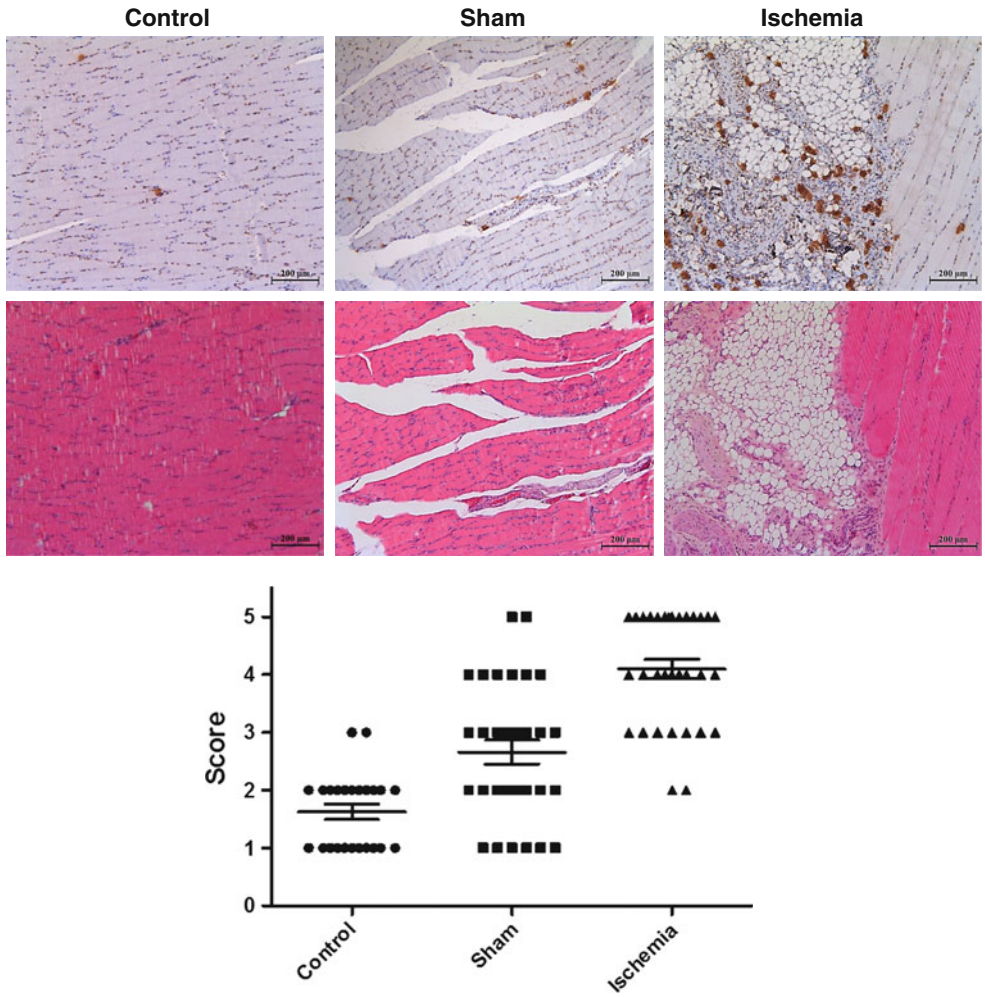

Fig. 8 The immunohistochemical results of a representative case under 10× lens (*top*). The quantified immuno-staining levels were plotted (*bottom*). The score of ischemic region was significantly higher than sham ($P < 10^{-4}$) and control region ($P < 10^{-8}$)

Conclusion

In the present study, the kinetic analysis of ^{68}Ga-NOTA-c (RGDyK) PET study was performed in rats with surgically induced forelimb ischemia. The metabolic stability was evaluated with the blood samples of two normal rats, and no significant metabolism has occurred. Dynamic PET data were obtained from thirteen rats during 120 min in the animal PET/CT scanner. To evaluate temporal changes of ischemic uptakes, the rats were scanned at 3, 5 and 7 days after ischemic surgery. However, temporal changes were not significant. The 3-compartment model with reversible binding and a variable blood volume fraction (3C5P) was shown to best describe the time activity curve of the ischemic region. The total distribution volume obtained from the 3C5P model shows reasonable agreement with two graphical analyses (Logan and RE plot). The uptake and distribution volumes of the ischemic region were 2–3 times higher than the sham operation and control regions, and these results were strongly supported by immunohistochemical analysis. In conclusion, the kinetic modeling studies with dynamic ^{68}Ga-NOTA-c(RGDyK) PET scan were feasible based on an image-derived input function in a rat ischemia model. In addition, the kinetic modeling analysis performed in this study will be useful for the quantitative evaluation of ^{68}Ga-NOTA-c(RGDyK) binding to $\alpha_v\beta_3$ in angiogenic tissues.

Acknowledgments This work was supported by Grants [2008-2003852, R31-10089 (WCU Program), 2011K000709, NRF-2012M2A2A7035853] from the National Research Foundation and the Converging Research Center Program funded by the Ministry of Education, Science, and Technology.

Conflict of interest The authors declare that they have no conflict of interest.

References

1. Veikkola T, Karkkainen M, Claesson-Welsh L, Alitalo K (2000) Regulation of angiogenesis via vascular endothelial growth factor receptors. Cancer Res 60(2):203–212
2. Carmeliet P (2005) Angiogenesis in life, disease and medicine. Nature 438(7070):932–936
3. Ferrara N, Kerbel RS (2005) Angiogenesis as a therapeutic target. Nature 438(7070):967–974
4. Hynes RO (2002) Integrins: bidirectional, allosteric signaling machines. Cell 110(6):673–687
5. Hood JD, Cheresh DA (2002) Role of integrins in cell invasion and migration. Nat Rev Cancer 2(2):91–100
6. Brooks PC, Montgomery AM, Rosenfeld M, Reisfeld RA, Hu T, Klier G, Cheresh DA (1994) Integrin $\alpha_v\beta_3$ antagonists promote tumor regression by inducing apoptosis of angiogenic blood vessels. Cell 79(7):1157–1164
7. Ruoslahti E (2002) Specialization of tumour vasculature. Nat Rev Cancer 2(2):83–90
8. Shimaoka M, Springer TA (2003) Therapeutic antagonists and conformational regulation of integrin function. Nat Rev Drug Discov 2(9):703–716
9. Haubner R, Weber WA, Beer AJ, Vabuliene E, Reim D, Sarbia M, Becker KF, Goebel M, Hein R, Wester HJ, Kessler H, Schwaiger M (2005) Noninvasive visualization of the activated αvβ3 integrin in cancer patients by positron emission tomography and [^{18}F]Galacto-RGD. PLoS Med 2(3):e70
10. Haubner R, Beer AJ, Wang H, Chen X (2010) Positron emission tomography tracers for imaging angiogenesis. Eur J Nucl Med Mol Imaging 37(Suppl 1):S86–S103
11. Yang J, Guo H, Miao Y (2010) Technetium-99 m-labeled Arg-Gly-Asp-conjugated alpha-melanocyte stimulating hormone hybrid peptides for human melanoma imaging. Nucl Med Biol 37(8):873–883
12. Yan Y, Chen K, Yang M, Sun X, Liu S, Chen X (2011) A new ^{18}F-labeled BBN-RGD peptide heterodimer with a symmetric linker for prostate cancer imaging. Amino Acids 41(2):439–447
13. Picchio M, Beck R, Haubner R, Seidl S, Machulla HJ, Johnson TD, Wester HJ, Reischl G, Schwaiger M, Piert M (2008) Intratumoral spatial distribution of hypoxia and angiogenesis assessed by ^{18}F-FAZA and ^{125}I-Gluco-RGD autoradiography. J Nucl Med 49(4):597–605
14. Liu Z, Yan Y, Liu S, Wang F, Chen X (2009) ^{18}F, ^{64}Cu, and ^{68}Ga labeled RGD-bombesin heterodimeric peptides for PET imaging of breast cancer. Bioconjug Chem 20(5):1016–1025
15. Yoshimoto M, Ogawa K, Washiyama K, Shikano N, Mori H, Amano R, Kawai K (2008) $\alpha_v\beta_3$ Integrin-targeting radionuclide therapy and imaging with monomeric RGD peptide. Int J Cancer 123(3):709–715
16. Guo N, Lang L, Li W, Kiesewetter DO, Gao H, Niu G, Xie Q, Chen X (2012) Quantitative analysis and comparison study of [^{18}F]AlF-NOTA-PRGD2, [^{18}F]FPPRGD2 and [^{68}Ga]Ga-NOTA-PRGD2 using a reference tissue model. PLoS One 7(5):e37506
17. Jacobson O, Zhu L, Niu G, Weiss ID, Szajek LP, Ma Y, Sun X, Yan Y, Kiesewetter DO, Liu S, Chen X (2011) MicroPET imaging of integrin $\alpha_v\beta_3$ expressing tumors using ^{89}Zr-RGD peptides. Mol Imaging Biol 13(6):1224–1233
18. Jeong JM, Hong MK, Chang YS, Lee YS, Kim YJ, Cheon GJ, Lee DS, Chung JK, Lee MC (2008) Preparation of a promising angiogenesis PET imaging agent: ^{68}Ga-labeled c(RGDyK)-isothiocyanatobenzyl-1,4,7-triazacyclononane-1,4,7-triacetic acid and feasibility studies in mice. J Nucl Med 49(5):830–836
19. Kim JH, Lee JS, Kang KW, Lee HY, Han SW, Kim TY, Lee YS, Jeong JM, Lee DS (2012) Whole-body distribution and radiation dosimetry of ^{68}Ga-NOTA-RGD, a positron emission tomography agent for angiogenesis imaging. Cancer Biother Radiopharm 27(1):65–71
20. Shetty D, Lee YS, Jeong JM (2010) ^{68}Ga-labeled radiopharmaceuticals for positron emission tomography. Nucl Med Mol Imaging 44(4):233–240
21. Breeman WA, Verbruggen AM (2007) The ^{68}Ge/^{68}Ga generator has high potential, but when can we use ^{68}Ga-labelled tracers in clinical routine? Eur J Nucl Med Mol Imaging 34(7):978–981
22. Beer AJ, Haubner R, Goebel M, Luderschmidt S, Spilker ME, Wester HJ, Weber WA, Schwaiger M (2005) Biodistribution and pharmacokinetics of the $\alpha_v\beta_3$-selective tracer ^{18}F-galacto-RGD in cancer patients. J Nucl Med 46(8):1333–1341
23. Ferl GZ, Dumont RA, Hildebrandt IJ, Armijo A, Haubner R, Reischl G, Su H, Weber WA, Huang SC (2009) Derivation of a compartmental model for quantifying ^{64}Cu-DOTA-RGD kinetics in tumor-bearing mice. J Nucl Med 50(2):250–258
24. Lee KH, Jung KH, Song SH, Kim DH, Lee BC, Sung HJ, Han YM, Choe YS, Chi DY, Kim BT (2005) Radiolabeled RGD uptake and α_v integrin expression is enhanced in ischemic murine hindlimbs. J Nucl Med 46(3):472–478
25. Wang Y, Seidel J, Tsui BM, Vaquero JJ, Pomper MG (2006) Performance evaluation of the GE healthcare eXplore VISTA dual-ring small-animal PET scanner. J Nucl Med 47(11):1891–1900
26. Nakamura Y, Tsuji M, Arai S, Ishihara C (1995) A method for rapid and complete substitution of the circulating erythrocytes in SCID mice with bovine erythrocytes and use of the substituted mice for bovine hemoprotozoa infections. J Immunol Methods 188(2):247–254
27. Logan J, Fowler JS, Volkow ND, Wang GJ, Ding YS, Alexoff DL (1996) Distribution volume ratios without blood sampling from graphical analysis of PET data. J Cereb Blood Flow Metab 16(5):834–840
28. Zhou Y, Ye W, Brasić JR, Crabb AH, Hilton J, Wong DF (2009) A consistent and efficient graphical analysis method to improve the quantification of reversible tracer binding in radioligand receptor dynamic PET studies. Neuroimage 44(3):661–670
29. Zhou Y, Ye W, Brasić JR, Wong DF (2010) Multi-graphical analysis of dynamic PET. Neuroimage 49(4):2947–2957
30. Kim SJ, Lee JS, Im KC, Kim SY, Park SA, Lee SJ, Oh SJ, Lee DS, Moon DH (2008) Kinetic modeling of 3′-deoxy-3′-^{18}F-fluorothymidine for quantitative cell proliferation imaging in subcutaneous tumor models in mice. J Nucl Med 49(12):2057–2066